frontiers | Frontiers in Marine Science

TYPE Original Research
PUBLISHED 18 September 2024
DOI 10.3389/fmars.2024.1440845

OPEN ACCESS

EDITED BY
Xianqing Lv,
Ocean University of China, China

REVIEWED BY
Yongchao Zhu,
Hefei University of Technology, China
Chuang Xu,
Guangdong University of Technology, China

*CORRESPONDENCE
Nengfang Chao
chaonf@cug.edu.cn

RECEIVED 30 May 2024
ACCEPTED 16 August 2024
PUBLISHED 18 September 2024

CITATION
Ma A, Chao N, Qin P, Hwang C, Zhu C, Chen G, Wang Z and Wang S (2024) Performance assessment of sentinel-3/6 altimeter data for marine gravity recovery. *Front. Mar. Sci.* 11:1440845. doi: 10.3389/fmars.2024.1440845

Performance assessment of sentinel-3/6 altimeter data for marine gravity recovery

Aoyu Ma[1], Nengfang Chao[1]*, Pengbo Qin[2], Cheinway Hwang[3], Chengcheng Zhu[4], Gang Chen[1], Zhengtao Wang[5] and Shuai Wang[6]

[1]Key Laboratory of Geological Survey and Evaluation of Ministry of Education, China Hubei Key Laboratory of Marine Geological Resources, China University of Geosciences, Wuhan, China, [2]Key Laboratory of Marine Mineral Resources, Guangzhou Marine Geological Survey, China Geological Survey, Guangzhou, China, [3]Department of Civil Engineering, National Yang Ming Chiao Tung University, Hsinchu, Taiwan, [4]School of Surveying and Geo-Informatics, Shandong Jianzhu University, Jinan, Shandong, China, [5]School of Geodesy and Geomatics, Key Laboratory of Geospace Environment and Geodesy, Wuhan University, Wuhan, China, [6]School of Geography and Information Engineering, China University of Geosciences (Wuhan), Wuhan, China

High-precision sea surface height is crucial for determining the marine gravity field. The Sentinel-3/6 altimetry missions, equipped with SRAL and Poseidon-4 altimeters, provide this essential data. However, there is a lack of comprehensive assessment of the Sentinel-3/6 altimeters for inverting marine gravity anomalies (MGA). In this study, we employ the inverse Venning-Meinsz method to derive nine sets of 1′×1′ MGAs in the South China Sea (SCS) and the Ross Sea (RS). Specifically, MGAs from Sentinel-3A, Sentinel-3B, Sentinel-6 SARM, Sentinel-6 LRM, HY-2A, ICESat-2, and CryoSat-2 are denoted as S3A, S3B, S6S, S6L, H2A, IS2, and CS2, respectively. MGA from the combined HY-2A, ICESat-2, and CryoSat-2 is referred to as HIC, while 3SHIC denotes the MGA from the combination of Sentinel-3/6 SARM, HY2A, ICESat-2, and CryoSat-2. We assess the performance of these MGAs using the EGM08, DTU17, SIO V32.1, and SDUST2021 gravity field models, as well as shipboard gravity across different ocean regions. Among the Sentinel-3/6 MGAs, S3B exhibits the highest accuracy in the SCS, with a root mean square error (RMSE) of 5.277 mGal, followed closely by S3A. Conversely, S3A demonstrates the highest accuracy with an RMSE of 4.635 mGal, followed by S3B in the RS. The inversion accuracy of MGAs from S6S and S6L are comparable, though S6S outperforms S6L in the open sea. The performance of MGAs from Sentinel-3/6 matches or surpasses that of other altimetry missions during the same period. In the SCS, the best-performing MGA is 3SHIC, with an RMSE of 4.585 mGal, closely matching DTU17. However, 3SHIC exhibits superior performance in the RS with an RMSE of 4.263 mGal compared to DTU17 and SDUST 2021. Furthermore, the performance of 3SHIC, which integrates Sentinel-3/6 data, improves that of HIC by 0.74% and 3.37% in the SCS and RS, respectively. These results underscore the contribution of

Sentinel-3/6 altimeters to the MGA, particularly in coastal and high-latitude regions. Integration of Sentinel-3/6 data with other altimetry satellites is expected to enhance the spatial resolution and accuracy of the global marine gravity field, especially with the successful establishment of the network of Sentinel-6 in the future.

KEYWORDS

sentinel-3/6, marine gravity anomalies, performance, South China Sea, Ross Sea

1 Introduction

High-precision marine gravity anomalies (MGA) are crucial for constructing a global earth gravity model and facilitating marine resource development (Hwang et al., 2002; Yang et al., 2018; Zhu et al., 2022). In recent decades, with the development of satellite altimetry technology, more than 20 altimetry satellites have been successfully launched, conducting geodetic missions (GM) and exact repeat missions (ERM). These missions gather significant altimetry data in marine regions, particularly in remote areas, and provide technology and data support for deriving high-resolution and high-accuracy marine gravity fields (Tziavos et al., 1998). With improvements in the precision and coverage of altimetry data, the accuracy of MGA increases (Chao et al., 2023; Sandwell et al., 2013; Sandwell, 1992). As a result, satellite altimetry is widely used to derive regional and global marine gravity fields (Chao et al., 2023; Guo et al., 2022; Sandwell et al., 2013, 2021; Zhang et al., 2017, 2022; Zhu et al., 2020, 2022, 2023).

The Sentinel-3/6 is currently employed in a variety of Earth scientific domains, with a specific focus on marine remote sensing (Bohn et al., 2022; Mishra et al., 2019) and inland water altimetry (An et al., 2022; Bergé-Nguyen et al., 2021; Donlon et al., 2021; Le Gac et al., 2021; Maiwald et al., 2020; Zhang et al., 2020). For example, Sentinel-3/6 altimetry data has been effectively used to quantify inland water levels (An et al., 2022; Bergé-Nguyen et al., 2021; Le Gac et al., 2021; Zhang et al., 2020), global sea level rise (Donlon et al., 2021), and ocean circulation (Maiwald et al., 2020). The Sentinel-3A altimetry system is very similar to the CryoSat-2 satellite. Following the launch of Sentinel-3B, the satellite was positioned in a cross-phase orbit with Sentinel-3A to achieve a denser coverage pattern. The observation data has a phase offset of ±140 degrees and a time discrepancy of 30 seconds (Aviso, 2022; Mertikas et al., 2020). The Sentinel-6A satellite has a newly designed Ku/C dual-band synthetic aperture radar Poseidon-4 altimeter. The Sentinel-3/6 has shown exceptional performance in orbit determination and sea surface height (SSH) measurement (Donlon et al., 2021; Yang et al., 2019). Altimetry satellites, such as HY-2A, ICESat-2, and CryoSat-2, are mainly used to construct global marine gravity field models (Chao et al., 2023; Sandwell et al., 2021; Wan et al., 2022; Zhu et al., 2022). There are few marine gravity fields derived from the Sentinel-3/6. While several studies (Liu et al., 2021; Yazid et al., 2022) have tried to inverse MGA by combining Sentinel-3/6 with other altimetry missions, there has been no comprehensive assessment of the reliability and accuracy of MGAs from Sentinel-3/6. In this study, we will use altimetry measurements from Sentinel-3/6, HY-2A/B, JASON-3, ICESat-2, CryoSat-2, and their various combinations to derive MGAs in the South China Sea (SCS) and Ross Sea (RS). This will allow for a thorough analysis of the performance of Sentinel-3/6 for determining MGAs in various regions.

The primary work of this study is as follows: 1) Editing shipboard gravity data to assess altimetry accuracy; 2) Combining SSH data from Sentinel-3/6, HY-2A, ICESat-2, and CryoSat-2 altimetry satellites to derive 1'×1' MGAs using the Inverse Venning-Meins (IVM) remove-restore method in the SCS and RS, and the MGAs from Sentinel-3/6 is compared with JASON-3 and HY-2B during the same period; 3) The performance of Sentinel-3/6 in deriving MGAs is assessed across the different ocean using the EGM08, DTU17, SIO V32.1, SDUST2021 gravity field models and data-edited shipboard gravity data, as well as the results from others various altimetry missions.

2 Study area

Figure 1 shows the region of the South China Sea ($104°E - 124°E$, $0°N - 28°N$) and the Ross Sea ($160°E - 180°E$, $60°S - 70°S$). The SCS covers roughly 3.3 million km^2 and has an extensive range of depths. The shallowest depths are located near the coast, while the deepest is found in the Manila Trench (up to 5,377 meters), with an average depth of around 1,212 meters (Hsiao et al., 2023; Li et al., 2001; Morton and Blackmore, 2001; Zhu et al., 2023). The RS is a deep bay in Antarctica's Southern Ocean. It is located north of the Ross Ice Shelf, between Victoria Land and Marie Byrd Land. The RS is the world's southernmost sea and one of the most southerly regions accessible by ship. It is also among the least affected by human activities on earth (Ballard et al., 2012). The SCS region has complicated topography, whereas the RS region has simpler geography and no large land masses. As a result, this study chose these two sample regions for research and thoroughly assessed the performance of Sentinel-3/6 for

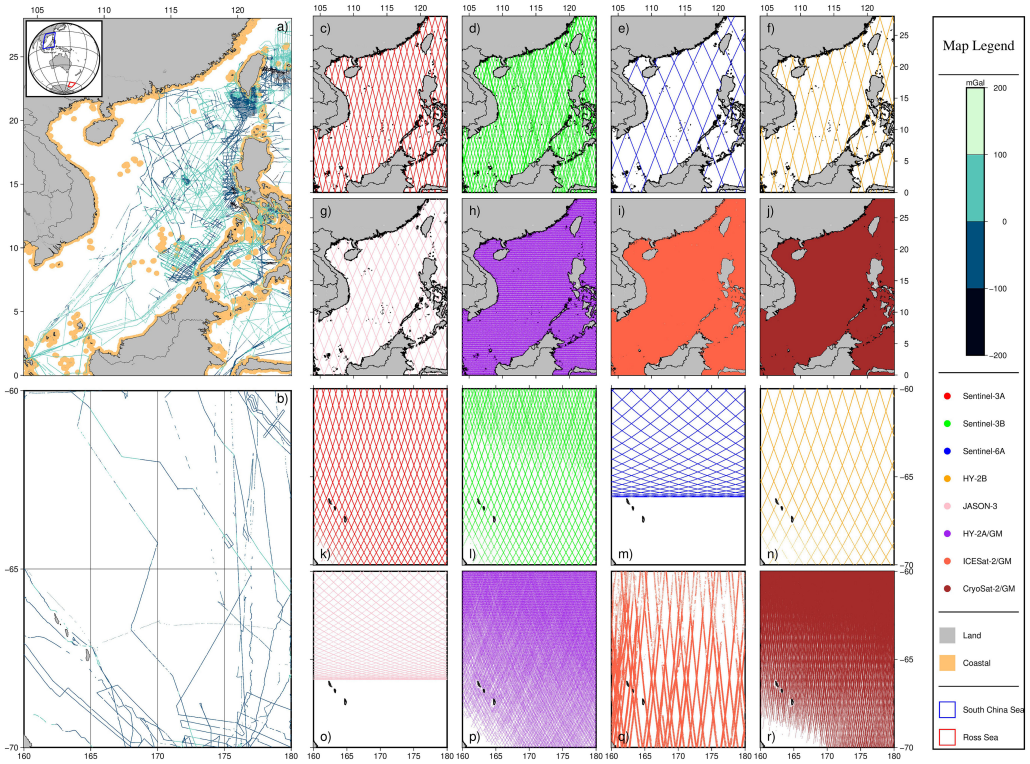

FIGURE 1
Study area and distribution of shipboard gravity and altimetry data in the SCS and RS. **(A, B)** Shipboard gravity distributions in the SCS and RS; **(C–J)** Track distributions of Sentinel-3A, Sentinel-3B, Sentinel-6A, HY-2A/B, JASON-3, ICESat-2, and CryoSat-2 in the SCS; **(K–R)** Track distributions of Sentinel-3A, Sentinel-3B, Sentinel-6A, HY-2A/B, JASON-3, ICESat-2, and CryoSat-2 in the RS.

inverting MGAs. The SCS region is further divided into coastal and open ocean for a comprehensive evaluation (Figure 1).

3 Data

3.1 Satellite altimetry data

3.1.1 Altimetry satellite

This study uses eight altimetry satellites: Sentinel-3A, Sentinel-3B, Sentinel-6A, HY-2A/B, JASON-3, ICESat-2, and CryoSat-2. Here, HY-2B and JASON-3 are included only for comparison with Sentinel-3/6 during the same mission type and period. Therefore, excluding HY-2B and JASON-3, the remaining altimetry data are used for independent and combined inversion MGAs. Figure 2 shows the launch dates and expected end of life for each satellite.

- Sentinel-3/6: Sentinel-3A was launched in February 2016, with an adjacent orbit spacing of 0.93°, an average orbit height of 815 km, and an orbital inclination of 98.65°. Sentinel-3B was launched in April 2018. Four months after launch, it was moved into the nominal orbit, which alternates with Sentinel-3A. This move caused a change in the cycle number for Sentinel-3B's data products. On November, 2018, Sentinel-3B was put in a crisscross orbit with Sentinel-3A, with their orbits planned to be "interleaved". This mode allows a more complete and uniform sampling of the Earth's surface, resulting in denser coverage. Sentinel-3B has the same orbital parameters as Sentinel-3A, but their phase difference is ±140°, with a 30-second observation gap (Mertikas et al., 2020). Sentinel-3 is equipped with a Synthetic Aperture Radar Altimeter that operates in the Ku/C dual-frequency band. It usually runs in Synthetic Aperture Radar Mode (SARM), with Low Resolution Mode (LRM) as a backup. Sentinel-6A was launched on November 21, 2020, while Sentinel-6B is planned to launch five years later. With an inclination of 66°, both spacecraft are high-inclination, non-sun-synchronous satellites. Sentinel-6A is equipped with the Poseidon-4 altimeter, which operates in the Ku/C dual frequency band. Poseidon-4's alternate time sequence measuring mode essentially doubles the number of SARM observations. Importantly, it enables simultaneous operation with LRM, removing the need to switch between LRM and SARM. As a result, altimetry data from Sentinel-3A and Sentinel-3B are acquired using SARM, but altimetry data from Sentinel-6A are obtained using both the SARM and the LRM of the altimeter (Aviso, 2024).
- HaiYang-2: On August 16, 2011, the Taiyuan Satellite Launch Centre successfully launched China's first marine dynamic environment satellite, the HY-2A. On March 23, 2016, the HY-2A satellite moved from its nominal orbit for ERM to a GM orbit. The new orbit is about 2 kilometers

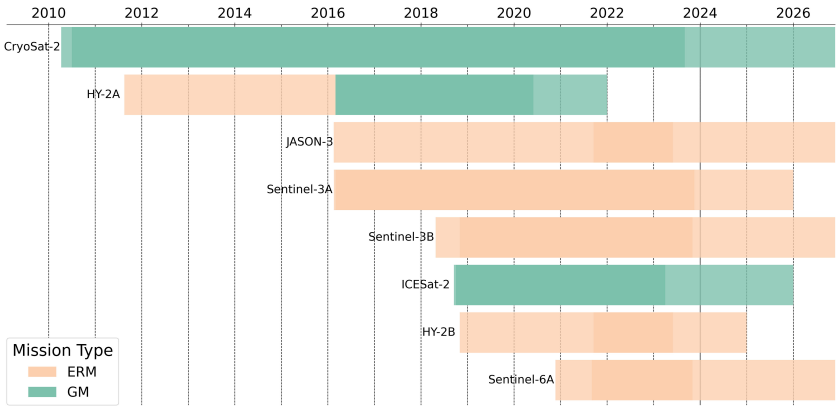

FIGURE 2
The launch dates and expected end of life of the altimetry satellites used in this study (with the opaque portion representing the data period used in this study, as shown in Table 1).

higher than the original, with a period of 168 days and an inclination of 99.3°. The HY-2A satellite carried GM until June 2020 (Figure 2). HY-2B is China's second ocean dynamic environment satellite, with an orbital altitude of 973 km and an inclination of 99.3°.

- JASON-3: JASON-3 was successfully launched on January 17, 2016. JASON-3 operates in a near-Earth orbit at an altitude of 1,336 km with an inclination of 66.05°. It is equipped with the Poseidon-3B Altimeter for ERM, which has a 9.9-day repetition period.
- ICESat-2: ICESat-2 was launched in September 2018 with the Advanced Topographic Laser Altimeter System. The satellite was supposed to be operational for three years, but it still works today. The satellite is intended to orbit at an altitude of 496 km and an inclination of 94°, making it a non-sun-synchronous satellite. It has a 91-day orbital cycle and a high altimetry accuracy of 0.1 meters. ICESat-2detects ground by emitting six beams grouped in pairs using diffractive optical components. Each pair is made up of a strong and a weak beam, with an energy ratio of around 4:1 between the two.
- CryoSat-2: CryoSat-2 was successfully launched in April 2010 and placed in a near-polar, non-sun-synchronous orbit with an average height of 717 km and an inclination of 92°. CryoSat-2 contains the SAR Interferometer Radar Altimeter for GM, which has a 369-day repetition period with 30-day sub-cycles. In July 2020, the European Space Agency modified the orbit of the CryoSat-2 satellite so that it would routinely match with the National Aeronautics and Space Administration's (NASA) ICESat-2 satellite. As a result, the number of cycles for data products has changed.

3.1.2 SSH data

The Sentinel-3/6, HY-2B, JASON-3, HY-2A/GM, and CryoSat-2/GM SSH data used in this study came from AVISO's non-time critical Level-2 Process sea level anomaly (SLA) data sets (Table 1).

TABLE 1 SSH Data Product Information.

Data	Period	Cycles	Documents Delivered Per Cycle	Measurement Mode	Data Sources
Sentinel-3A	2016.03-2023.11	001-105	770	SAR	AVISO
Sentinel-3B	2018.11-2023.11	009-085	770	SAR	AVISO
Sentinel-6hr	2021.09-2023.11	032-110	254	SAR	AVISO
Sentinel-6lr	2021.09-2023.11	032-110	254	LRM	AVISO
HY-2B*	2021.09-2023.06	076-119	Fluid	–	AVISO
JASON-3*	2021.09-2023.06	206-340	254	SAR	AVISO
HY-2A/GM	2016.03-2020-06	118-288	Fluid	–	AVISO
CryoSat-2/GM	2010.07-2023.09	007-245	Fluid	LRM	AVISO
ICESat-2/GM	2018.10-2023.04	–	–	–	NASA

*To compare the MGAs from Sentinel-3/6, HY-2B, and JASON-3during the same period, only a subset of data from HY-2B and JASON-3was selected.

The product is created by subtracting the mean sea surface (MSS) from the SSH and applying several modifications to the SLA data. The SLA data product is in NetCDF format and includes the correction values required to compute the SLA. It also offers the MSS using the combined SIO/CNES-CLS-15/DTU15 mean sea level reference over 20 years. Valid SSH data may be derived from SLA data products using Equation 1 (Aviso, 2024; Hsiao et al., 2023).

$$SSH = SLA + MSS \quad (1)$$

The ICESat-2/GM SSH data used in this study came from NASA's L3A-ALT12 product. Level-3A product is an along-track data product that has received numerous modifications and scene classifications from the Level 2 product. ATL12 primarily records data from open ocean regions, excluding areas covered by ice and interior water bodies. The SSH data is saved in HDF5 format, with each file having data from three strong and three weak beams. It is crucial to note that the beam locations of the strong and weak beams vary twice a year as a result of ICESat-2's solar panel illumination optimization. In this work, MGA is derived using six beam sets of ICESat-2 SSH data (Morison et al., 2022).

3.2 The global geopotential models

The EGM2008 geopotential model builds upon the EGM96 model by incorporating GRACE data, along with further processed satellite altimetry data and ground-based gravity data. It has a global grid resolution of 5'5'. The EGM2008 model achieves an approximation accuracy to the geoid of 11.1 cm globally (with China excluded from the testing area), with an approximation accuracy of around 14 cm in China. This model is used to compute the EGM2008 geoid model and the EGM2008 gravity field model, with the former used for the extraction of along-track residual geoid gradients to remove the long wavelength component of gravity anomalies, and the latter used for the restoration of residual gravity anomalies derived from the IVM method.

EICEN-6C4 is a global model produced by the German Research Centre for Geosciences in 2014, with a total of 2190 spherical harmonic coefficients. It primarily uses GRACE data, full GOCE data, and DTU10 topographic data. It is widely used in scientific research such as the gravity field (Förste et al., 2011). EICEN-6C4 outperforms EGM2008 in areas that have poor terrestrial data coverage. The EICEN-6C4 geopotential model was used to calculate the EICEN-6C4 gravity field model, which was used to filter shipboard gravity data using the triple-median error principle (Ince et al., 2019). Both geopotential models were downloaded from the International Center for Global Earth Models.

3.3 Mean dynamic topography

The sea surface topography is separated into two parts: time-varying topography (the distance between the instantaneous sea level and the MSS) and mean dynamic topography (MDT), which is the distance between the MSS and the geoid. In this research, we use the DTU22 MDT (https://ftp.space.dtu.dk/pub/DTU22/MDT/) provided by the Technical University of Denmark (DTU), which is calculated from the DTU21 MSS and the XG M2019e geoid (Knudsen et al., 2022).

3.4 Assessing data

In this study, we compare the accuracy of MGAs determined through altimetry with shipboard gravity and published global marine gravity field models. The shipboard gravity data were received from the National Centers for Environmental Information, and they included 69 tracks from 1967 to 2010 in the SCS and 23 tracks from 1961 to 2017 in the RS. The global marine gravity field is using the latest DTU17 model released by DTU (https://ftp.space.dtu.dk/pub/DTU17/1_MIN/) (Andersen and Knudsen, 2020), SDUST2021 released by Shandong University of Science and Technology (SDUST) (https://doi.org/10.5281/zenodo.6668159) (Zhu et al., 2022), and SIO V32.1 developed by Scripps Institution of Oceanography (SIO) (https://topex.ucsd.edu/pub/global_grav_1min/) (Sandwell et al., 2014). SIO V32.1 is currently recognized as one of the best marine gravity field models.

4 MGA inversion and assessment methods

In this study, we calculate MGA from altimetry data using remove-restore IVM. Firstly, the SSH model is obtained by summing up the EGM08 geoid model and DTU22 MDT. The along-track residual geoid gradients are derived by performing along-track processing on both the SSH model and the satellite altimetry SSH data, followed by differencing them. Then, using the Least Squares Collocation (LSC) method to calculate the gridded residual deflection of the vertical (DOV) component. The residual gravity anomaly and innermost zone gravity anomaly are calculated using the IVM formula. Finally, the residual gravity anomalies, innermost zone gravity anomalies, and the EGM08 gravity anomaly model are stacked to generate the final gravity anomalies seen in Figure 3.

Following the above computation steps, the 1'×1' MGA grids were derived from Sentinel-3A, Sentinel-3B, Sentinel-6 SARM, Sentinel-6 LRM, HY2A/GM, ICESat-2/GM and CryoSat-2/GM, and denoted S3A, S3B, S6S, S6L, H2A, IS2, CS2, respectively. The HIC is the result of an inversion by a combination of the HY2A, ICESat-2, and CryoSat-2. The 3SHIC is the result of a combined inversion of HY2A/GM, ICESat-2/GM, CryoSat-2/GM, Sentinel-3A, Sentinel-3B, and Sentinel-6 SARM data. The Sentinel-6 SARM altimetry data and the Sentinel-6 LRM altimetry data have the same trajectory but the former is more accurate than the latter (Jiang et al., 2023). And the inclusion of redundant input data increases calculation time. Therefore, Sentinel-6 LRM altimetry data are not employed in deriving 3SHIC. We combine data from all the above altimetry missions except HY-2B and JASON-3, as the purpose of using HY-2B and JASON-3 is to assess the potential of

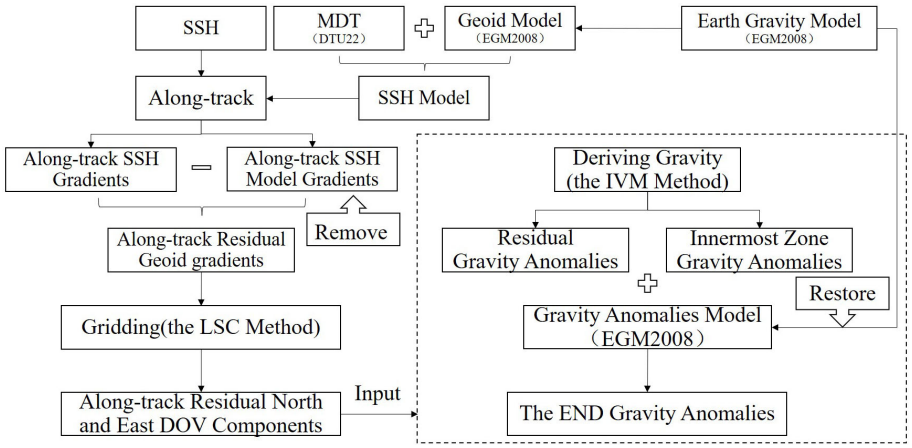

FIGURE 3
Flowchart of MGA from altimetry observations.

Sentinel-3/6 in recovering marine gravity during the same mission type and period.

4.1 Inverse Venning-Meinsz method

Along-track processing is carried out on SSH data from satellite altimetry and the model (MDT and geoid models combined). The difference between the two results in the residual geoid gradient, which is also the residual DOV at the crossover point. The residual gravity anomaly is calculated by applying the IVM formula to the east and north components of the residual DOV. Here, we directly present the IVM formula revised by Hwang (Hwang and Parsons, 1996):

$$\Delta g(p) = \frac{\gamma_0}{4\pi} \iint_{\sigma} H'(\xi_q \cos \alpha_{qp} + \eta_q \sin \alpha_{qp}) d\sigma_q \tag{2}$$

In the Equation 2, γ_0 is the mean gravity, $H'$is the derivative of the integration kernel function, p is the calculation point, q is the moving point, α_{qp} is the azimuth angle from the moving point q to the calculation point p, ξ_q is the north component of the DOV at the moving point, and η_q is the east component of the DOV at the moving point.

Azimuth angle α_{qp} is calculated by Equation 3:

$$\tan \alpha_{qp} = \frac{-\cos \varphi_p \sin (\lambda_q - \lambda_p)}{\cos \varphi_q \sin \varphi_p - \sin \varphi_q \cos \varphi_p \cos (\lambda_q - \lambda_p)} \tag{3}$$

The key to the IVM method is to discover an appropriate kernel function, which Hwang defines as

$$H(\psi_{\mathrm{pq}}) = \frac{1}{\sin \frac{\psi_{\mathrm{pq}}}{2}} + \log \left(\frac{\sin^3 \frac{\psi_{\mathrm{pq}}}{2}}{1 + \sin \frac{\psi_{\mathrm{pq}}}{2}} \right) \tag{4}$$

The derivation of Equation 4 gives Equation 5:

$$H' = \frac{dH}{d\psi_{\mathrm{pq}}} = -\frac{\cos \frac{\psi_{\mathrm{pq}}}{2}}{2 \sin^2 \frac{\psi_{\mathrm{pq}}}{2}} + \frac{\cos \frac{\psi_{\mathrm{pq}}}{2} (3 + 2 \sin \frac{\psi_{\mathrm{pq}}}{2})}{2 \sin^2 \frac{\psi_{\mathrm{pq}}}{2} (1 + \sin \frac{\psi_{\mathrm{pq}}}{2})} \tag{5}$$

The formula for the spherical distance ψ_{pq} between the calculation point p and the moving point q is given by Equation 6:

$$\cos \psi_{pq} = \sin \varphi_p \sin \varphi_q + \cos \varphi_p \cos \varphi_q \cos (\lambda_q - \lambda_p) \tag{6}$$

To prevent the spherical distance ψ_{pq} from reaching zero, gravity anomalies are often not calculated directly in the innermost zone. To avoid losing gravity anomalies in the innermost zone, the innermost zone effect must be taken into account while calculating gravity anomalies using the IVM method. To obtain the final residual gravity anomaly, the innermost zone gravity anomaly g_0 must be added to $\Delta g(p)$. The gravity anomalies in the innermost zone are calculated using Equation 7. ξ_x and η_y are the rates of change for the north and the east components of the grid's residual DOV, respectively. $s_0 = \sqrt{\frac{\Delta x \Delta y}{\pi}}$ is the innermost zone size, Δx and Δy are the grid intervals for the residual DOV in the east and north directions, respectively (Guo et al., 2023b).

$$g_0 = (s_0 \gamma_0 / 2)(\xi_x + \eta_y), \tag{7}$$

4.2 Editing of shipboard gravity data

To obtain a more dependable shipboard gravity, the following process was used: 1) The gravity discrepancies are calculated by subtracting the shipboard gravity values from the gravity model. These discrepancies are then compared to the mean of the gravity differences to exclude data points that are over three times the standard deviation. 2) The filtered gravity discrepancies are fitted with a polynomial equation. Shipborne points with gravity discrepancies exceeding three times the standard error after fitting is removed (Zhu et al., 2020). 3) The SIO V32.1 model is derived only from satellite altimetry data. Therefore, this gravity anomaly model is regarded as independent of shipboard gravity anomalies. It is used to reduce outliers from shipboard gravity anomaly data (Guo et al., 2023a). The shipboard gravity data were compared with the SIO V32.1 model, and only the shipboard gravity data with

differences within 10 mGal of the model gravity were retained (Figures 1A, B).

4.3 Accuracy assessment

The standard deviation (STD) represents the degree of dispersion across individuals within a group, and the root mean square error (RMSE) measures the departure of an observation from its true value. As a result, this research uses STD and RMSE to measure accuracy:

$$STD = \sqrt{\frac{\sum_{i=1}^{n}(Y_i - mean)^2}{n}} \tag{8}$$

$$RMSE = \sqrt{\frac{\sum_{i=1}^{n}(Y_i - Y_{real})^2}{n}} \tag{9}$$

In the Equations 8, 9, Y_i represents the ith value in the dataset. For STD, the "mean" is the average of all values, while for RMSE, Y_{real} denotes the actual value corresponding to Y_i. Both formulas use n to signify the total number of values.

5 Results

5.1 Edited shipboard gravity data

In this study, we use shipboard gravity data after editing to evaluate the accuracy of the altimetry-derived gravity field. The initial shipboard data for the SCS consisted of 69 lines and 467,972 data points. Following data editing, the shipboard data had 64 survey lines, which were reduced to 417,046 points with an outlier removal rate of 10.88%. The STD of the shipboard gravity data decreased from 45.663 mGal to 41.168 mGal (Figure 4). The initial shipboard data for the RS consisted of 23 lines and 87,733 data points. After data editing, the shipboard data retained 23 survey lines, reduced to 81,366 points, with an outlier removal rate of 7.25%. The STD of the shipboard gravity data decreased from 34.803 mGal to 24.754 mGal (Figure 4).

5.2 Comparisons of MGA from sentinel-3/6, HY-2B, and JASON-3during the same period in the SCS/RS

We compared the MGAs from HY-2B, JASON-3, and Sentinel-3/6 over the same period. Using five sets of SSH data from September 2021 to June 2023, we inverted MGA grids named S3A_S, S3B_S, S6S_S, H2B_S, and JS3_S. As shown in Table 2, the accuracy of the MGAs is approximately 5.3 mGal, and 4.7 mGal in the SCS and RS, respectively.

In the SCS and RS, the S3A_S demonstrates the highest accuracy (RMSE of 5.292 mGal and 4.719 mGal, respectively), surpassing both H2B_S and JS3_S. While S3A_S is more accurate than S3B_S, the overall accuracy of S3A is lower than S3B. This discrepancy is likely due to the absence of data from the Sentinel-3B orbit change period, which would have increased the track density of Sentinel-3B. Although the S3B_S inversion accuracy in the SCS is lower than JS3_S, it is superior to JS3_S in the RS. Overall, during the same period, Sentinel-3/6 demonstrated excellent performance in inverting MGA compared to other altimetry satellites with the same mission type.

5.3 Performance of MGA from sentinel-3/6 in the SCS/RS

The nine sets of MGA fields derived from altimetry, EGM08, DTU17, and SDUST2021, were assessed with data-edited shipboard

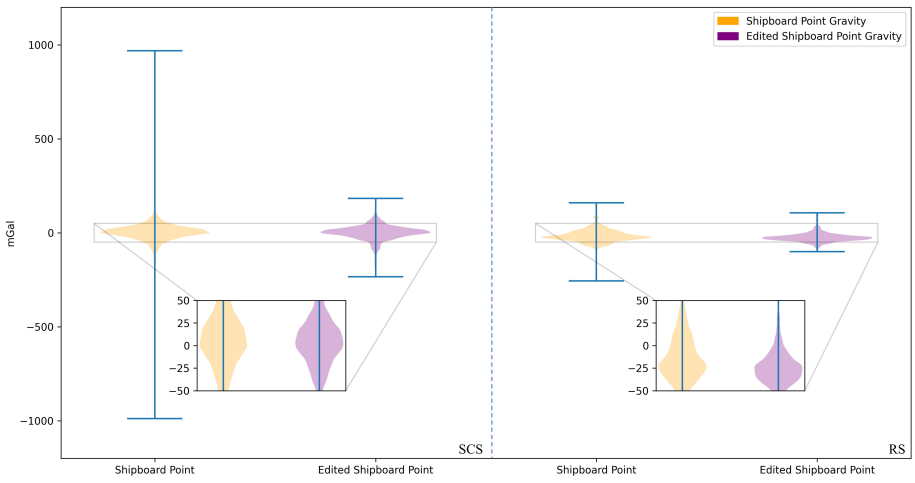

FIGURE 4
Before and after editing of shipboard data in the SCS and RS.

TABLE 2 Evaluation of MGA from altimetry and gravity field model using shipboard and SIO V32.1 data (Units: mGal).

Gravity Field	Shipboard in SCS STD/RMSE	Model in SCS STD/RMSE	Shipboard in RS STD/RMSE	Model in RS STD/RMSE
S3A_S	5.288/5.292	4.752/4.752	4.713/4.719	3.709/3.709
S3B_S	5.318/5.320	4.759/4.759	4.730/4.734	3.707/3.707
S6S_S	5.324/5.325	4.827/4.828	4.746/4.751	3.716/3.716
H2B_S	5.341/5.346	4.905/4.905	4.754/4.758	3.736/3.736
JS3_S	5.301/5.302	4.812/4.812	4.743/4.748	3.727/3.727

gravity data, respectively. Because SIO V32.1 is used for shipboard data editing, it is not included in the accuracy evaluation of the shipboard data. Instead, the nine sets of gravity fields derived from altimetry were compared with SIO V32.1 to assess the performance of MGA (Table 3).

EGM08 is the lowest accuracy in the SCS, with an RMSE of 5.329 mGal. The highest accuracy gravity field accuracy was 3SHIC, which was obtained by combined inversion of HY2A/GM, ICESat-2/GM, CryoSat-2/GM, Sentinel-3A, Sentinel-3B, and Sentinel-6A SARM (Figure 5A), with an RMSE of 4.585 mGal. The HIC accuracy of the gravity field using the combined inversion of HY2A/GM, ICESat-2/GM, and CryoSat-2/GM is 4.619 mGal, with a total accuracy of 3.882 mGal. The 3SHIC increases accuracy by 0.74% over the HIC. Among the MGAs in the SCS from independent individual altimetry data, CS2 has the best precision (RMSE of 4.763 mGal), while S6S/L has the lowest accuracy. Among the four SCS MGAs derived from independent individual altimetry data in Sentinel-3/6, S3B has the highest inversion accuracy (RMSE of 5.277 mGal), and S3A is the second highest. The inversion accuracies of S6S and S6L are nearly identical, with the overall accuracy of S6S being slightly higher than that of S6L.

In the RS, EGM08 has the lowest accuracy, with an RMSE of 4.788 mGal. 3SHIC (Figure 5B) has the highest accuracy, with an RMSE of 4.263 mGal, which is better than DTU17. 3SHIC has a 3.38% increase in accuracy over HIC. Among MGAs in the RS produced from independent individual altimetry data, CS2 has the best accuracy (RMSE of 4.560 mGal), while S6S/L has the lowest. Among Sentinel-3/6's four independent individual MGAs in the RS, S3A has the greatest performance (RMSE = 4.635 mGal), S3B is second, and S6S is superior to S6L.

The nine sets of MGAs from altimetry were evaluated for accuracy with shipboard gravity and SIO V32.1, respectively. The results show that the assessment of shipboard data is mostly compatible with those of SIO V32.1 (Figure 5C). The derived gravity field of the altimetry data, DTU17, and SDUST2021 (RS area) are all restored to the EGM08 gravity field model using the remove-restore method. They are extensions and refinements of the EGM08 gravity field model. The accuracy should be higher than EGM08. MGAs derived from the GM altimetry data are better than the Sentinel-3/6 by 0.3-0.7 mGal in the SCS. The main reason is the limited coverage and sparse tracks of ERM data in the study area. However, Sentinel-3A/B data overcomes the above limitations, and its capacity to calculate the marine gravity field is superior to that of HY2A/GM and ICESat-2/GM data in the RS. 3SHIC outperforms HIC in both SCS and RS, indicating that Sentinel-3/6 helps to derive the marine gravity field, particularly in the RS. According to

TABLE 3 Evaluation of MGA from altimetry and gravity field model using shipboard and SIO V32.1 data (Units: mGal).

Gravity Field	Shipboard in SCS STD/RMSE	Model in SCS STD/RMSE	Shipboard in RS STD/RMSE	Model in RS STD/RMSE
S3A	5.285/5.289	4.734/4.734	4.629/4.635	3.658/3.658
S3B	5.275/5.277	4.693/4.693	4.660/4.663	3.641/3.642
S6S	5.324/5.325	4.828/4.828	4.748/4.752	3.716/3.717
S6L	5.323/5.324	4.843/4.843	4.754/4.758	3.727/3.727
H2A	5.017/5.019	4.430/4.430	4.688/4.693	3.692/3.692
IS2	4.855/4.856	4.206/4.207	4.770/4.776	3.865/3.865
CS2	4.761/4.763	4.092/4.092	4.555/4.560	3.538/3.538
HIC	4.618/4.619	3.882/3.882	4.406/4.412	3.516/3.516
3SHIC	4.583/4.585	3.840/3.841	4.259/4.263	3.401/3.401
SDUST2021	4.272/4.272	–	4.417/4.422	–
EGM08	5.326/5.329	–	4.784/4.788	–
DTU17	4.548/4.551	–	4.324/4.328	–

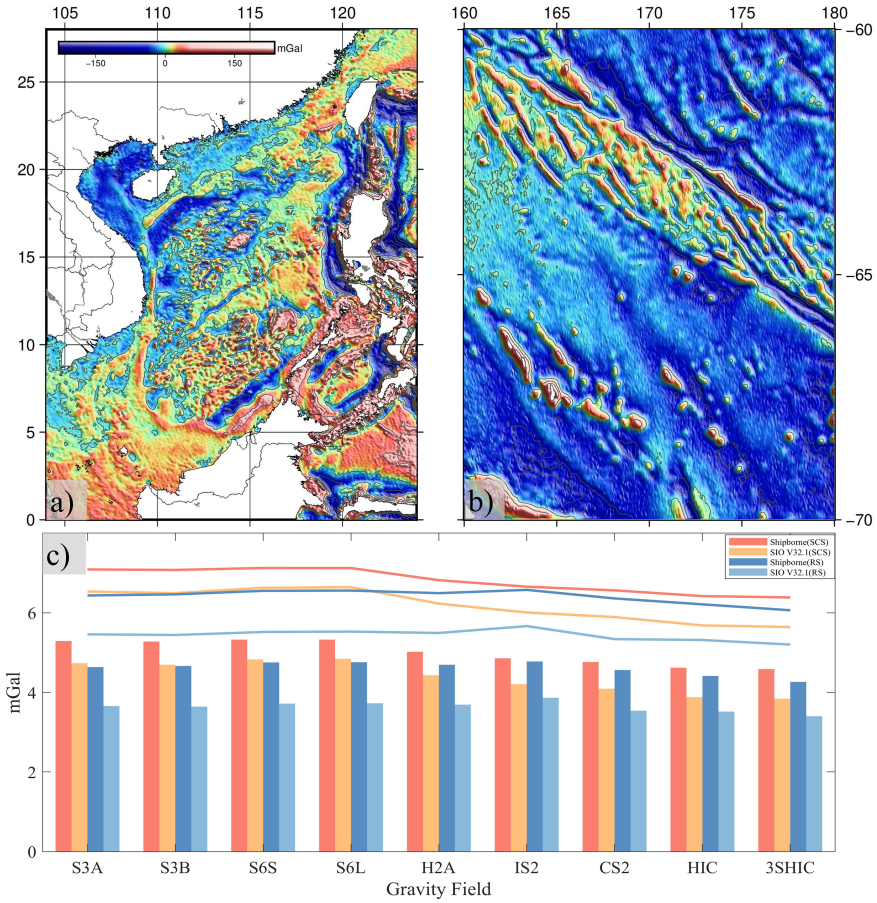

FIGURE 5
(A) 3SHIC gravity field in the SCS; **(B)** 3SHIC gravity field in the SCS; **(C)** RMSE of shipboard comparison with SIO V32.1.

Figure 1, Sentinel-6A's track density is much lower than that of Sentinel-3A/B. Sentinel-6A surveys the sea surface more accurately than Sentinel-3 (Jiang et al., 2023). However, both S3A and S3B outperform S6S and S6L, indicating that track density has a bigger impact on gravity field accuracy than range accuracy.

5.4 Performance of MGA from sentinel-3/6 with a single shipboard track in the SCS/RS

In Figure 6A, the green point indicates the RMSE's minimal value (RMSE_min), and the orange point indicates the RMSE's maximum value (RMSE_max). In the SCS and RS, the RMSE of a single shipboard survey line with nine sets of MGAs range from 2 mGal to 12 mGal. Among them, the range between the RMSE_min and RMSE_max values for lines v3614 in the SCS and elt32 in the RS is relatively small. This indicates that their RMSE shows more consistency compared to the other lines. In the SCS, the RMSE variations of the nine sets of MGAs are primarily in the range of 3-7 mGal for each line, with eight lines having RMSE_min more than 7 mGal (mainly in the Philippine offshore). In the RS, individual line RMSE fluctuations are primarily in the 2.5-6 mGal, with just one line having an RMSE_min more than 7 mGal. In general, the accuracy of the 9-group MGAs in the RS is higher than in the SCS. This can be attributed to the SCS's diverse geography, whereas the RS is mainly an open sea.

Figure 6B shows that the nine sets of MGAs in the SCS and RS areas are generally in agreement. This indicates that the Sentinel-3/6 could be used to determine MGA. In Figure 6A, the discrete points correspond to shipboard lines with RMSE_min larger than 7 mGal, which are not regarded as outliers to be deleted. The reason for this is that the edited shipboard data are deemed sufficiently credible and the comparatively limited capability of altimetry data to derive gravity in near-shore locations. The mean and median lines of the RS are generally smaller than those of the SCS, while the number of discrete points of the RS is also less than that of the SCS. This indicates that the accuracy of the inversion results in the RS is superior to that in the SCS.

5.5 Performance of MGA from Sentinel-3/6 over different region of the SCS

The SCS is separated into two different regions (coastal and distant-sea) to ensure that altimetry-derived MGAs are comprehensively assessed. The coastal region is defined as the outside edge of the coastal sea zone, spanning 12 nautical miles parallel to and outward (about 22 kilometers, as shown in

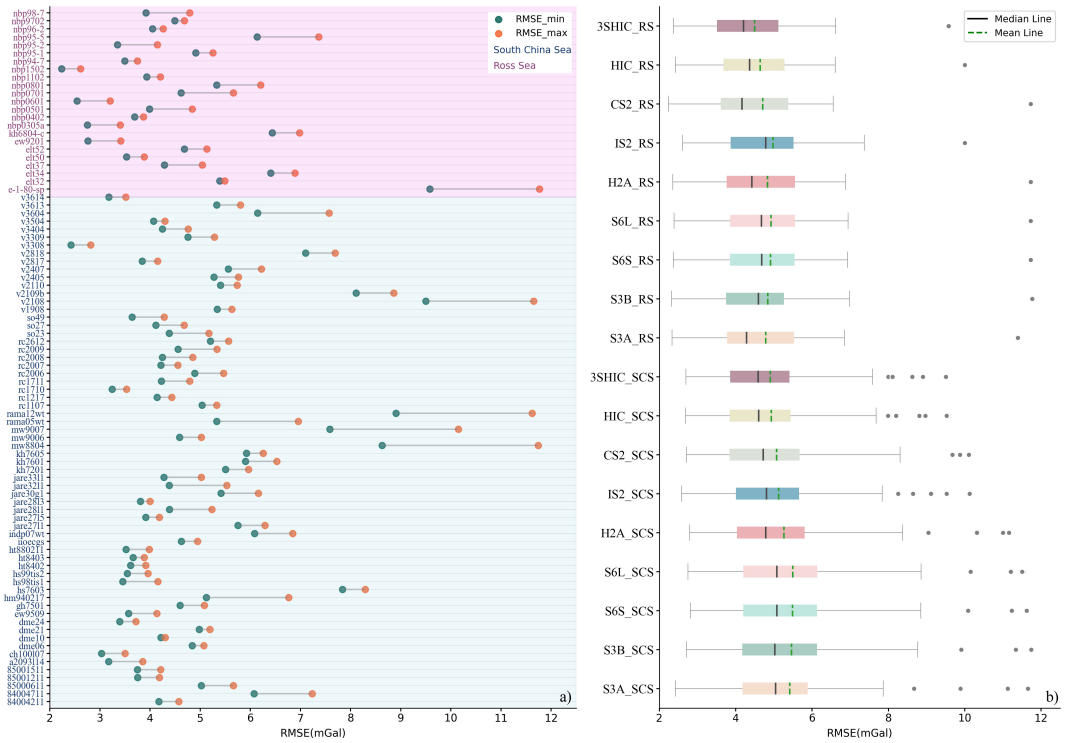

FIGURE 6
Accuracy analysis of nine sets of MGAs in the SCS and RS areas with each shipboard line. **(A)** the RMSE lollipop plot of a single shipboard line with nine sets of MGAs; **(B)** the RMSE box plot of a single shipboard line with nine sets of MGAs.

Figure 1A). As shown in Table 3 and Table 4, the outcomes of the regional assessment are generally consistent with the overall assessment. Table 4 shows that the coastal shipboard/model RMSE is generally higher than the distant-sea shipboard/model RMSE. This is because of near-shore altimetry data's limited ability to derive the gravity field. S6S is more accurate than S6L in the distant-sea region, but both are equally accurate in the coastal region. When all other parameters remain constant, it is concluded that the capacity to calculate the gravity field from Sentinel-6A SARM altimetry data in the distant-sea region outperforms that of the LRM. S3A and S3B display similar accuracies in the coastal region, while the latter is more accurate in the distant-sea region.

In the distant-sea region, 3SHIC's accuracy is nearly identical to that of DTU17. In the coastal region, the former is superior to the latter. The 3SHIC accuracy improves when compared to the HIC accuracy in both coastal and distant-sea locations, with the coastal region showing a 1.15% improvement. This indicates that the capability of Sentinel-3/6 altimetry data in deriving MGA is stronger in coastal region.

TABLE 4 Assessment of MGA from altimetry and gravity field model with shipboard data and SIO V32.1 in the coastal/distant-sea (Units: mGal).

Gravity Field	Coastal Shipboard	Distant-sea shipboard	Coastal Model	Distant-sea Model
S3A	7.330	4.387	7.796	2.666
S3B	7.335	4.366	7.736	2.635
S6S	7.379	4.418	7.953	2.717
S6L	7.372	4.420	7.979	2.725
H2A	6.820	4.240	7.336	2.447
IS2	6.479	4.167	6.893	2.410
CS2	6.382	4.072	6.786	2.250
HIC	6.107	3.992	6.416	2.160
3SHIC	6.037	3.975	6.347	2.138
SDUST2021	5.589	3.724	–	–
EGM08	7.354	4.438	–	–
DTU17	6.065	3.909	–	–

6 Discussion

Satellite altimetry data from GM utilizes unrepeated track measurements, while ERM utilizes repeated track measurements. The resolution of GM data is an order of magnitude higher than that of ERM data. Increasing track density can significantly enhance the accuracy of the gravity field. As a result, GM data are usually more accurate in deriving MGA fields than ERM data. Although constructing a geoid/gravity anomaly grid can mitigate the inherent along-track resolution of satellites to some extent. The insufficient orbital density of altimetry data still leads to large areas in S3A, S3B, S6S, and S6L where gravity information is filled using the EGM08 model rather than directly derived from actual altimetry data. The

MGA accuracy obtained by combining multi-source satellite altimetry data surpasses that of any single altimetry satellite, further supporting the aforementioned assertion. However, the track density of Sentinel-3A/B data is lower than that of HY2A/GM and ICESat-2/GM data in the RS. The accuracy of the derived MGA from Sentinel-3A/B surpasses that of HY2A/GM and ICESat-2/GM. The accuracy of MGA from Sentinel-3A/B is higher than that using HY-2B and JASON-3during the same period in the RS. 3SHIC is the most precise gravity field grid in the RS, which combines Sentinel-3A/B data. These indicate that Sentinel-3/6 has significant potential for improving the derived MGA field in the high latitude area.

In this study, the performance of 3SHIC generally aligns with that of SDUST2021. In the SCS, 3SHIC's accuracy is slightly lower than SDUST2021 (with RMSE values of 4.585 mGal and 4.272 mGal, respectively). However, 3SHIC exhibits better accuracy (with RMSE values of 4.263 mGal and 4.422 mGal, respectively) in the RS. SDUST2021 employs the latest XGM2019e geopotential model for 'remove-restore' in the SCS and the EGM2008 geopotential model in the RS (Zhu et al., 2022). The 3SHIC in this study uses the EGM2008 geopotential model for both regions. SDUST2021 uses a higher number of altimetry satellite data than 3SHIC. The SCS has a more complicated topography than RS which is primarily made up of open ocean. In situations of complicated topography, using data from many satellites to derive MGA often leads to greater inversion accuracy than data from a single satellite, but its improvement is limited in open ocean region. Based on the RS region assessment, Sentinel-3A/B altimetry data likely contribute to 3SHIC outperforming SDUST2021. Therefore, we will further integrate Sentinel-3A/B and other altimetry data to construct a global MGA field model in the future.

7 Conclusion

To assess the performance of MGA from Sentinel-3/6, nine sets of 1'×1' MGAs in the SCS and RS were inverted using the IVM method. The accuracy of MGA was conducted using data-edited shipboard gravity and the global marine gravity field models. The results indicate that Sentinel-3/6 satellites possess the capability to derive MGA, with a stronger ability in coastal regions. Sentinel-3A/B altimetry data outperform Sentinel-6 SARM/LRM in deriving the gravity field, as well as HY2A/GM and ICESat-2/GM altimetry data in the RS. The performance of MGA from Sentinel-3/6 data matches or surpasses that of HY-2B and JASON-3 during the same period. In the open ocean, Sentinel-6A SARM altimetry data outperforms LRM in deriving MGA. Sentinel-3A/B altimetry data show great potential for improving the MGA field derived in high latitudes.

Improving the track density and range accuracy of altimetry data could significantly enhance the accuracy of the calculated MGA. And increasing track density has a greater impact than improving ranging accuracy. While the capability of independent Sentinel-3/6 to derive the marine gravity field is not exceptional, their combination with other altimetry missions has a greater effect. Sentinel-6 was originally scheduled to do GM. As Sentinel-6B has not yet been launched, Sentinel-6A is currently operating in ERM. Once Sentinel-6 is successfully deployed and transitions to GM operations, the track density of Sentinel-3/6 altimetry data will see a notable increase. Combined with Sentinel-6's high range accuracy, this will significantly contribute to the global marine gravity field. As a result, the combined Sentinel-3/6 data will significantly increase the accuracy of MGA.

Data availability statement

The original contributions presented in the study are included in the article/supplementary material. Further inquiries can be directed to the corresponding authors.

Author contributions

AM: Visualization, Validation, Software, Investigation, Formal analysis, Data curation, Conceptualization, Writing – review & editing, Writing – original draft. NC: Writing – original draft, Project administration, Writing – review & editing, Supervision, Resources, Funding acquisition, Conceptualization. PQ: Supervision, Funding acquisition, Writing – review & editing. CH: Writing – review & editing, Supervision, Software, Resources, Methodology. CZ: Writing – review & editing, Supervision. GC: Writing – review & editing, Supervision, Project administration. ZW: Writing – review & editing, Supervision, Project administration. SW: Writing – review & editing, Data curation.

Funding

The author(s) declare financial support was received for the research, authorship, and/or publication of this article. This study was supported by the National Natural Science Foundation of China (NSFC) under Grants 42274115, 41974019, and 42274003; the National Science Foundation for Outstanding Young Scholars (No. 42122025); and the Opening Fund of the Key Laboratory of Geological Survey and Evaluation of the Ministry of Education (Grant Nos. GLAB2022ZR04 and GLAB2023ZR04).

Acknowledgments

The authors thank the following data providers for making the data available: Sentinel-3/6, HY-2A/B, JASON-3, and CryoSat-2 non-time critical Level 2 Process SLA products from AVISO, ICESat-2 L3A-ALT12 SSH data from NASA, shipborne gravity data from the National Centers for Environmental Information), the global marine gravity field model SIO V32.1 from SIO, and the global marine gravity field model DTU 17 from DTU.

Conflict of interest

The authors declare that the research was conducted in the absence of any commercial or financial relationships that could be construed as a potential conflict of interest.

Publisher's note

References

An, Z., Chen, P., Tang, F., Yang, X., Wang, R., and Wang, Z. (2022). Evaluating the performance of seven ongoing satellite altimetry missions for measuring inland water levels of the great lakes. *Sensors*. 22 (24), 9718. doi: 10.3390/s22249718

Andersen, O. B., and Knudsen, P. (2020). The DTU17 global marine gravity field: First validation results. *Proc.* 2020-1-1, 2020. Springer.

Aviso (2022). *Sentinel-3/ Jason-CS-Sentinel-6 L2P SLA Product Handbook*. Available online at: https://www.aviso.altimetry.fr/fileadmin/documents/data/tools/hdbk_L2P_S3_S6.pdf (accessed February, 2024).

Aviso (2024). *Along-track Level-2+ (L2P) Sea Level Anomaly Sentinel-3 / Jason-CS-Sentinel-6 Product Handbook*. Available online at: https://www.aviso.altimetry.fr/fileadmin/documents/data/tools/hdbk_L2P_S3_S6.pdf (accessed February, 2024).

Ballard, G., Jongsomjit, D., Veloz, S. D., and Ainley, D. G. (2012). Coexistence of mesopredators in an intact polar ocean ecosystem: The basis for defining a Ross Sea marine protected area. *Biol. Conserv.* 156, 72–82. doi: 10.1016/j.biocon.2011.11.017

Bergé-Nguyen, M., Cretaux, J. F., Calmant, S., Fleury, S., Satylkanov, R., Chontoev, D., et al. (2021). Mapping mean lake surface from satellite altimetry and GPS kinematic surveys. *Adv. Space Res.* 67 (3), 985–1001. doi: 10.1016/j.asr.2020.11.001

Bohn, N., Di Mauro, B., Colombo, R., Thompson, D. R., Susiluoto, J., Carmon, N., et al. (2022). Glacier ice surface properties in south-west Greenland ice sheet: first estimates from PRISMA imaging spectroscopy data. *J. Geophys. Res. Biogeosci.* 127 (3). doi: 10.1029/2021JG006718

Chao, N. F., Wang, S., Ouyang, G. C., Hwang, C., Jin, T. Y., Zhu, C. C., et al. (2023). An improved triple collocation-based integration of multiple gravity anomaly grids from satellite altimetry: Contribution of ICESat-2. *Remote Sens. Environ.* 292. doi: 10.1016/j.rse.2023.113582

Donlon, C. J., Cullen, R., Giulicchi, L., Vuilleumier, P., Francis, C. R., Kuschnerus, M., et al. (2021). The Copernicus Sentinel-6 mission: Enhanced continuity of satellite sea level measurements from space. *Remote Sens. Environ.* 258. doi: 10.1016/j.rse.2021.112395

Förste, C., Bruinsma, S., Flechtner, F., Abrykosov, O., Dahle, C., Marty, J., et al. (2011). EIGEN-6C3 - The latest Combined Global Gravity Field Model including GOCE data up to degree and order 1949 of GFZ Potsdam and GRGS Toulouse. Proceedings of; 2011-1-1 2011.

Guo, J., Luo, H., Zhu, C., Ji, H., Li, G., and Liu, X. (2022). Accuracy comparison of marine gravity derived from HY-2A/GM and CryoSat-2 altimetry data: a case study in the Gulf of Mexico. *Geophys J. Int.* 230 (2), 1267–1279. doi: 10.1093/gji/ggac114

Guo, J., Zhang, H., Li, Z., Zhu, C., Liu, X., and Luo, H. (2023a). Joint reprocessing of shipborne gravity anomalies based on multiSources:A case study of the gulf of Mexico. *Geomatics and Information Science of Wuhan University*. 0 (0). doi: 10.13203/j.whugis20230088

Guo, J., Zhu, F., Xin, L., and Xiaotao, C. (2023b). Time-varying marine gravity of Bay of Bengal derived from CryoSat-2 altimetry data. *Huazhong Keji Daxue Xuebao (Ziran Kexue Ban)/Journal Huazhong Univ. Sci. Technol. (Natural Sci. Edition)* 51, 85–91.

Hsiao, Y., Hwang, C., Chen, T., and Cho, Y. (2023). Assessing models of sea level rise and mean sea surface with sentinel-3B and Jason-3 altimeter data near Taiwan: impacts of data quality and length. *Remote Sens (Basel)* 15, 3640. doi: 10.3390/rs15143640

Hwang, C., Hsu, H., and Jang, R. (2002). Global mean sea surface and marine gravity anomaly from multi-satellite altimetry: applications of deflection-geoid and inverse Vening Meinesz formulae. *J. Geod* 76, 407–418. doi: 10.1007/s00190-002-0265-6

Hwang, C., and Parsons, B. (1996). An optimal procedure for deriving marine gravity from multi-satellite altimetry. *Geophys J. Int.* 125, 705–718. doi: 10.1111/gji.1996.125.issue-3

Ince, E. S., Barthelmes, F., Reißland, S., Elger, K., Förste, C., Flechtner, F., et al. (2019). ICGEM–15 years of successful collection and distribution of global gravitational models, associated services, and future plans. *Earth Syst. Sci. Data* 11 (2), 647–674. doi: 10.5194/essd-11-647-2019

Jiang, M., Xu, K., and Wang, J. (2023). *Evaluation of Sentinel-6 Altimetry Data over Ocean Remote Sensing*. 15 pp. Reprinted.

Knudsen, P., Andersen, O. B., Maximenko, N., and Hafner, J. (2022). A new combined mean dynamic topography model–DTUUH22MDT. *Proc.* 2022-1-1, 2022.

Le Gac, S., Boy, F., Blumstein, D., Lasson, L., and Picot, N. (2021). Benefits of the Open-Loop Tracking Command (OLTC): Extending conventional nadir altimetry to inland waters monitoring. *Adv. Space Res.* 68 (2), 843–852. doi: 10.1016/j.asr.2019.10.031

Li, J., Ning, J., Chen, J., and Chao, D. (2001). Determination of gravity anomalies over the South China Sea by combination of TOPEX/Poseidon, ERS2 and Geosat altimeter data. *Acta Geodaetica Et Cartographica Sin.* 30, 197–202.

Liu, S. W., Li, Y. L., Sun, Q. T., Wan, J. H., Jiao, Y., and Jiang, J. H. (2021). Evaluation of marine gravity anomaly calculation accuracy by multi-source satellite altimetry data. *Front. Earth Sci.* 9. doi: 10.3389/feart.2021.730777

Maiwald, F., Brown, S. T., Koch, T., Milligan, L., Kangaslahti, P., Schlecht, E., et al. (2020). Completion of the AMR-C instrument for sentinel-6. *IEEE J. Sel Top. Appl. Earth Observ. Remote Sens.* 13, 1811–1818. doi: 10.1109/JSTARS.2020.2991175

Mertikas, S., Tripolitsiotis, A., Donlon, C., Mavrocordatos, C., Féménias, P., Borde, F., et al. (2020). The ESA Permanent Facility for altimetry calibration: Monitoring performance of radar altimeters for Sentinel-3A, Sentinel-3B and Jason-3 using transponder and sea-surface calibrations with FRM standards. *Remote Sens.* 12 (16), 2642. doi: 10.3390/rs12162642

Mishra, S., Stumpf, R. P., Schaeffer, B. A., Werdell, P. J., Loftin, K. A., and Meredith, A. (2019). Measurement of cyanobacterial bloom magnitude using satellite remote sensing. *Sci. Rep.* 9. doi: 10.1038/s41598-019-54453-y

Morison, J., Hancock, D., Dickinson, S., Robbins, J., Roberts, L., Kwok, R., et al. (2022). Ice, cloud, and land elevation satellite (ICESat-2) project algorithm theoretical basis document (ATBD) for ocean surface height. doi: 10.5067/E5JD7G9RZNUI

Morton, B., and Blackmore, G. (2001). South China Sea. *Mar. pollut. Bull.* 42, 1236–1263. doi: 10.1016/S0025-326X(01)00240-5

Sandwell, D., Garcia, E., Soofi, K., Wessel, P., Chandler, M., and Smith, W. H. (2013). Toward 1-mGal accuracy in global marine gravity from CryoSat-2, Envisat, and Jason-1. *Leading Edge* 32 (8), 892–899. doi: 10.1190/tle32080892.1

Sandwell, D. T. (1992). Antarctic marine gravity field from high-density satellite altimetry. *Geophys J. Int.* 109, 437–448. doi: 10.1111/gji.1992.109.issue-2

Sandwell, D. T., Harper, H., Tozer, B., and Smith, W. H. F. (2021). Gravity field recovery from geodetic altimeter missions. *Adv. Space Res.* 68, 1059–1072. doi: 10.1016/j.asr.2019.09.011

Sandwell, D. T., Müller, R. D., Smith, W., Garcia, E., and Francis, R. (2014). New global marine gravity model from CryoSat-2 and Jason-1 reveals buried tectonic structure. *Science* 346 (6205), 65–67. doi: 10.1126/science.1258213

Tziavos, I. N., Sideris, M. G., and Forsberg, R. (1998). Combined satellite altimetry and shipborne gravimetry data processing. *Mar. Geod* 21, 299–317. doi: 10.1080/01490419809388144

Wan, X., Hao, R., Jia, Y., Wu, X., Wang, Y., and Feng, L. (2022). Global marine gravity anomalies from multi-satellite altimeter data. *Earth Planets Space* 74 (1), 165. doi: 10.1186/s40623-022-01720-4

Yang, J., Jekeli, C., and Liu, L. (2018). Seafloor topography estimation from gravity gradients using simulated annealing. *J. Geophysical Research: Solid Earth* 123, 6958–6975. doi: 10.1029/2018JB015883

Yang, J. G., Zhang, J., and Wang, C. Y. (2019). Sentinel-3A SRAL global statistical assessment and cross-calibration with Jason-3. *Remote Sens (Basel)* 11. doi: 10.3390/rs11131573

Yazid, N. M., Din, A. H. M., Omar, A. H., et al. (2022). Optimised gravity anomaly fields from along-track multi-mission satellite altimeter over Malaysian seas. *Terrestrial Atmospheric Oceanic Sci.* 33, 1. doi: 10.1007/s44195-022-00003-5

Zhang, S., Sandwell, D. T., Jin, T., and Li, D. (2017). Inversion of marine gravity anomalies over southeastern China seas from multi-satellite altimeter vertical deflections. *J. Appl. Geophy* 137, 128–137. doi: 10.1016/j.jappgeo.2016.12.014

Zhang, S., Zhou, R., Jia, Y., et al. (2022). Performance of HaiYang-2 altimetric data in marine gravity research and a new global marine gravity model NSOAS22. *Remote Sens (Basel)* 14, 4322. doi: 10.3390/rs14174322

Zhang, X. X., Jiang, L. G., Kittel, C., et al. (2020). On the performance of sentinel-3 altimetry over new reservoirs: approaches to determine onboard *A priori* elevation. *Geophys Res. Lett.* 47. doi: 10.1029/2020GL088770

Zhu, C., Guo, J., Gao, J., et al. (2020). Marine gravity determined from multi-satellite GM/ERM altimeter data over the South China Sea: SCSGA V1.0. *J. Geod* 94, 50.

Zhu, C., Guo, J., Yuan, J., Li, Z., Liu, X., and Gao, J. (2022). SDUST2021GRA: global marine gravity anomaly model recovered from Ka-band and Ku-band satellite altimeter data. *Earth Syst. Sci. Data* 14 (10), 4589–4606. doi: 10.5194/essd-14-4589-2022

Zhu, C., Yang, L., Bian, H., et al. (2023). Recovering gravity from satellite altimetry data using deep learning network. *IEEE Trans. Geosci Remote Sens.* doi: 10.1109/TGRS.2023.3280261